Multi-decadal analysis of root-zone soil moisture applying the exponential filter across CONUS

Kenneth J. Tobin[1], Roberto Torres[1], Wade T. Crow[2], and Marvin E. Bennett[1]

[1] Texas A&M International University, Center for Earth and Environmental Studies, Laredo, Texas, United States

[2] United States Department of Agriculture, Agricultural Research Service Hydrology and Remote Sensing Laboratory, Beltsville, Maryland, United States

Correspondence to: Kenneth J. Tobin (ktobin@tamiu.edu)

Abstract. This study applied the exponential filter to produce an estimate of root-zone soil moisture (RZSM). Four types of microwave-based, surface satellite soil moisture were used. The core remotely sensed data for this study came from NASA's long lasting AMSR-E mission. Additionally three other products were obtained from the European Space Agency Climate Change Initiative (CCI). These datasets were blended based on all available satellite observations (CCI-Active; CCI-Passive; CCI-Combined). All of these products were quarter degree and daily. We applied the filter to produce a soil moisture index (SWI) that others have successfully used to estimate RZSM. The only unknown in this approach was the characteristic time of soil moisture variation (T). We examined five different eras (1997-2002; 2002-2005; 2005-2008; 2008-2011; 2011-2014) that represented periods with different satellite data sensors. SWI values were compared with *in situ* soil moisture data from the International Soil Moisture Network at a depth ranging from 20 to 25 cm. Selected networks included the U.S. Department of Energy Atmospheric Radiation Measurement (ARM) program (25 cm), Soil Climate Analysis Network (SCAN; 20.32 cm), SNOwpack TELemetry (SNOTEL; 20.32 cm), and the U.S. Climate Reference Network (USCRN; 20 cm). We selected *in situ* stations that had reasonable completeness. These datasets were used to filter out periods with freezing temperatures and rainfall using data from the Parameter elevation Regression on Independent Slopes Model (PRISM). Additionally, we only examined sites where surface and root zone soil moisture had a reasonable high lagged r-value ($r>0.5$).

The unknown T value was constrained based on two approaches: optimization of root mean square error (RSME) and calculation based on the NDVI value. Both approaches yielded comparable results; although, as to be expected, the optimization approach generally outperformed NDVI based estimates. Best results were noted at stations that had an absolute bias within 10%. SWI estimates were more impacted by the *in situ* network than the

surface satellite product used to drive the exponential filter. Average Nash-Sutcliffe coefficients (NS) for ARM ranged from -0.1 to 0.3 and were similar to the results obtained from the USCRN network (0.2 to 0.3). NS values from the SCAN and SNOTEL networks were slightly higher (0.1 to 0.5). These results indicated that this approach had some skill in providing an estimate of RZSM. In terms of root mean square error (RMSE; in volumetric soil moisture) ARM values actually outperformed those from other networks (0.02 to 0.04). SCAN and USCRN RMSE average values ranged from 0.04 to 0.06 and SNOTEL average RMSE values were higher ranging (0.05 to 0.07). These values were close to 0.04, which is the baseline value for accuracy designated for many satellite soil moisture missions.

1 Introduction

Soil moisture is one of the most difficult hydrologic variables to either monitor or model (Lattenmaier et al., 2015). Understanding soil moisture dynamics is critical to support many diverse applications in hydrology, meteorology, and agriculture. In the agricultural sector a fundamental limiting factor that constrains crop productivity is root zone soil moisture (RZSM). Understanding root zone moisture dynamics is important also from a water resource standpoint and is a valuable measure in drought monitoring (Bolten et al., 2010; Bolten and Crow, 2012). The dimensions of RZSM also impact other systems beyond the hydrologic cycle, most notably with the quantification of carbon fluxes within soils. Therefore, direct sensing of RZSM dynamics will bring us closer to a truer understanding of the carbon soil pool, with obvious implications for future climate change.

Given the importance of RZSM to agricultural and other applications, more effort is needed to understand the impacts of climate change associated with this critical variable. The National Aeronautics and Space Administration (NASA), European Space Agency (ESA), and other governments across the world have had a long history of supporting missions that generate remotely sensed surface soil moisture, including the Scanning Multichannel Microwave Radiometer (SMMR), the Special Sensor Microwave Imager (SSM/I), Tropical Rainfall Measurement Mission (TRMM), Advanced Microwave Scanning Radiometer-Earth Observing System (AMSR-E), Soil Moisture and Ocean Salinity (SMOS), Soil Moisture Active Passive (SMAP), scatterometers on the European Remote Sensing satellites, which includes (SCAT) and the Advanced Scatterometer (ASCAT) to name only a few (*e.g.* Lakshmi et al. 1997; Wagner et al. 1999; Kerr et al. 2001; Jackson et al. 2002; Hutichson, 2003; Njoku et al, 2003; McCabe et al. 2005; Owe et al., 2008; Entekhabi et al., 2010). Passive microwave soil moisture estimate, like

AMSR-E measured the horizontal and vertical polarization temperatures in several wavelengths, which include: 6.6/6.9 GHz (C-band), and 10.7 GHz (X-band), 19.3 GHz (Ku-band). In addition, the vertical polarization is examined at 36.5/37.0 GHz (Ka-band). An advantage of the more recent SMOS and SMAP missions is that they operate at a lower frequency 1.2/1.4 GHz (L-band), which has great penetrative power, especially in highly vegetated areas. In terms of the active sensors both SCAT and ASCAT operated at 5.3 GHz (C-band) and have a similar design philosophy. These sensors make sequential observations of the backscattering coefficient with six sideways looking antennas and make sequential observations of the backscattering coefficient using three polarizing antennas.

Liu et al, (2012) described the development of two extensively validated surface soil moisture products. These products were created using a harmonized dataset based on all available soil moisture retrievals; one from the Vienna University of Technology (TU Wien) based on active microwave observations (Wagner *et al.*, 2003, Bartalis *et al.*, 2007) and one from the Vrije Universiteit Amsterdam (VUA), in collaboration with NASA Goddard Space Flight Center Hydrological Sciences Laboratory, based on passive microwave observations (Owe *et al.*, 2008). This effort was a part of the ESA Climate Change Initiative (CCI). The harmonization of these datasets incorporated the advantages of both microwave techniques and spanned the entire period from 1978 onward. This effort is unlike NOAA's Soil Moisture Operational Products System (SMOPS), which was a long-term record of soil moisture based on only passive microwave data.

A long-standing goal of the soil remote sensing community is to develop techniques that can observe changes in RZSM at depths greater than 10 cm, because all of the missions described above are confined to sensing moisture only within the top 5 cm of the profile. In 2015 NASA launched the SMAP mission that had the potential to combine of the advantages of passive and active microwave retrievals to estimate soil moisture dynamics at depth. Unfortunately, early during this mission the satellite's radar failed. Despite this setback NASA had invested considerable resources into the development of an Ensemble Kalman Filter (EnKF)-based Level 4 RZSM product for SMAP (Reichle et al., 2016) and the development of lower-frequency airborne radar systems for deeper penetration of the soil column (via the EV-1 AirMOSS project). While this work is to be commended, the limited time availability of these products precludes their use for long-term climatic trend studies.

This study used the exponential filter to leverage the longer duration CCI surface soil moisture record to produce a record of RZSM that can be compared over almost two decades (1997-2014). Wagner et al. (1999)

developed the exponential filter to examine soil moisture trends from ERS Scatterometer data focusing on the Ukraine. A later refinement of this filter included the development of a recursive version that had the virtue of a greater ease of implementation (Albergel et al, 2008). In recent years several authors have produced RZSM estimates using the exponential filter and have conduct comparisons at a range of spatial scales (Ford et al. 2014; Manfredaet al. 2014; Qiu et al. 2014; Peterson et al. 2014; Kedzior and Zawadzki, 2016). At the heart of the exponential filter method is the assumption of hydrologic equilibrium within the soil profile that makes it possible to estimate RZSM by using only surface measurements, provided that soil physical properties are known. This method also assumes that there is no loss from the root zone due to transpiration. Transfer of soil moisture from the surface to the root zone is controlled by a pseudodiffusivity term that allows both positive and negative fluxes from and to the deep layer. This approach overcame a limitation of the EnKF approach in that data assimilation is not dependent on obtaining data from a land surface model, in which there can be significant uncertainty in terms of the model parameters used to constrain water and energy balances (Kumar et al, 2009). This study presents the results of the application of the exponential filter produced using four satellite soil moisture products from 1997-2014 focusing on Continental United States (CONUS). As such this work represents a unique application of the exponential filter over a mutlidecadal time scale, which is only afforded by the long duration CCI record.

2 Data

2.1 Era Definitions

The data examined in this study spans over 17 years. As such we compared soil moisture produced by the exponential filter over five, roughly equal eras (3-4.5 year), which were defined based on the available satellite retrievals during each era (see Liu et al. 2012). These eras included: November 27 1997-June 18 2002 (pre-AMSR-E), June 19 2002-June 30 2005 (Early AMSR-E), July 1 2005-June 30 2008 (Middle AMSR-E), July 1 2008-October 3 2011 (Late AMSR-E), and October 4 2011-December 31, 2014 (post-AMSR-E; Table 1). The pre-AMSR-E era relied heavily on the TRMM Microwave Imager (TMI) passive observations and SCAT active retrievals that operated until 2006. In fact, the climatology of the passive dataset during this period was rescaled based on TMI data and likewise the same was true of AMSR-E during eras 2-4. During the Early AMSR-E era passive observations from the Windsat satellite came on line (Gaiser 2004). The Middle AMSR-E era was a time of transition in terms of active observations as the SCAT satellite is replaced by ASCAT. The Late AMSR-E era saw

111 the arrival of the ESA SMOS mission. After the failure of AMSR-E, SMOS observations took on a more prominent
112 role within the CCI passive microwave framework. Also during the post-AMSR-E the Japanese Space Agency
113 launched AMSR2 (Wentz et al. 2014), which is considered the replacement for the long lasting AMSR-E mission.

114 **2.2 In Situ Soil Moisture**

115 Direct, *in situ* comparisons were made between RZSM estimates with *in situ* data from the International Soil
116 Moisture Network (ISMN; Dorigo et al., 2011). The ISMN provides access to a host of meteorological and soil
117 moisture data (at many depths). In this study, we selected soil moisture at two depths. Surface soil (0-10 cm) and
118 RZSM (20-25 cm) moisture was compared to assess the performance of the exponential filter method. In this study
119 we focused on four networks within CONUS that have been examined in previous studies. Al Bitar et al. (2012)
120 conducted an extensive evaluation of SMOS data using two networks we utilized: the Soil Climate Analysis
121 Network (SCAN; 20.32 cm) and SNOwpack TELemetry (SNOTEL; 20.32 cm). Additionally, we obtained soil
122 moisture observations from two other CONUS networks: the U.S. Department of Energy Atmospheric Radiation
123 Measurement (ARM; 25 cm) program (Jackson et al 1999) and the U.S. Climate Reference Network (USCRN; 20
124 cm; Bell et al., 2013). Complete ARM observations only existed from eras 1 to 4 and USCRN data was available for
125 only era 5 (Table 1). *In situ* values were aggregated to a daily time step (based on UTC time) that matched the
126 surface satellite-based soil moisture product described below. Figures 1 and 2 show the location of the stations
127 selected across the five eras.

128 The ARM network used the Campbell Scientific1 229-L heat dissipation matric potential sensor to estimate
129 soil moisture (Reece 1996). Calibration of this method was based on comparison of matric potential with soil water
130 release curves (Klute, 1986). Conversely, the SCAN, SNOTEL, and USCRN networks all used a Stevens Water
131 Hydra Probe (Schaefer et al., 2007; Bell et al., 2013). Seyfried et al. (2005) described the calibration approach and
132 how the dielectric measurements from the Hydra Probe sensor were converted into volumetric soil moisture
133 measurements.

134 **2.3 Surface Satellite-Based Soil Moisture**

135 This study was supported by four surface (5 cm) soil moisture products, three of which came from the CCI program.
136 We used the CCI Passive, CCI Active, and CCI Combined products (Version 03.1). The harmonization process

involved in the creation of these products was described by Liu et al. (2012) and these datasets are available on-line (http://www.esa-soilmoisture-cci.org/node/145). In addition, we also utilized stand-alone data from the AMSR-E mission during eras 2-4. In this study we acquired the version produced by the Land Surface Parameter Model (LPRM; Owe et al. 2008; ftp://hydrol.sci.gsfc.nasa.gov/data/s4pa/WAOB). All of these satellite soil moisture products were produced at a daily time step with a 0.25^{o} spatial resolution.

2.4 Other Datasets

Several other dataset were used in an ancillary role. Air temperature and precipitation data were obtained from Parameter elevation Regression on Independent Slopes Model (PRISM; Daly et al. 1994) from grid cells (4 km spatial resolution) co-located with examined *in situ* sites (PRISM Climate Group 2015). These data were used to screen dates below freezing and with significant precipitation data, as suggested by (Dorigo et al., 2011), to enhance quality control.

In addition, Normalized Difference Vegetation Index (NDVI) values (Tucker 1979) were used to help constrain the only unknown in the exponential filter, the characteristic time length and was derived from Moderate Resolution Imagining Spectroradiometer (MODIS) data. The version of MODIS (MOD13Q1) used near-infrared reflectances that were atmospherically corrected to mask water, clouds, aerosols and cloud shadows. Datasets were provided in a sinusoidal grid with a 250 m resolution and an average of nine pixels around each *in situ* station were used to calculate a global average NVDI for each era.

3 Methods

3.1 Initial Station Filtering

To ensure selection of the highest quality *in situ* stations, we applied two criteria in our initial station selection. The first criterion involved the amount of missing data within a candidate station. Sites that had an excessive number of missing data, a total of over 20 days per year, were rejected. A second criterion related to a fundamental assumption of the exponential filter method, which is that there is a hydrologic connection between the surface and root zone horizons. One would expect that deeper within the profile there would be a greater lag in response. Therefore, a lagged r-value between surface measurements (generally made at 5 cm) and root zone data from 20 to 25 cm depth was made. Root zone lag was calculated between 1 to 40 days and the day with the highest lagged r-value was

selected. Stations whose maximum lagged r-value fell below 0.5 were rejected. Qiu et al. (2014) used a similar selection criterion in their study.

3.2 Exponential Filter

Wagner et al. (1999) originally developed the exponential filter and Albergel et al. (2008) refined this approach with a more robust recursive version of this method. This version provided an estimate of a soil wetness index (SWI) within the root zone. This index standardized RZSM based on the total range of values recorded by the *in situ* dataset. The recursive formulation provided a predictor of RZSM at time (t_n), which in this study was given in days, and was derived as:

$$SWI_{mn} = SWI_{mn(n-1)} + K_n [ms (t_n) - SWI_{mn(n-1}] \quad (1)$$

where $SWI_{mn(n-1)}$ represented the estimated RZSM at time t_{n-1}, ms (t_n) was the surface soil moisture estimate based on either CCI products or AMSR-E retrievals, and K_n was the gain at time t_n determined with:

$$K_n = \frac{K_{n-1}}{K_{n-1} + e^{\frac{t_n - t_{n-1}}{T}}} \quad (2)$$

where T represented the timescale of soil moisture variation in days. At the beginning of each era and after excessively large gaps in ms (t_n) data (> 12 days) the filter was initialized with $SWI_{m(1)}$ = ms (t_n) and K_{n1} set to one. Results from a data denial experiment described below provided support for the selection of 12 days as an appropriate timescale to reset the filter. The prime advantage of the exponential filter was that the only unknown was T. Finally, the SWI_{mn} generated from the exponential filter, which ranged from 0 to 1.000, was rescaled to match the range of the *in situ* data (in volumetric units) allowing for comparisons between these datasets.

3.3 Objective Metrics

Direct comparisons were made between CONUS *in situ* stations that represented a long-time series. While it is true that soil moisture measurements exhibit a high degree of spatial variability over a wide range of spatial scales from field plot to watershed (*e.g*, Western *et al*., 2004; Wilson *et al*., 2004; Brocca *et al*., 2007) temporal variation is much more muted. Temporal stability is a concept fully rooted in soil science (Vachaud et al., 1985; Martinez-Fernandez and Ceballos, 2003). Therefore, the approach of this study was to use standard objective metrics such as

lagged r-values to describe the relationship between (coarse-scale) of root zone soil moisture estimates based on the exponential filter and (point-scale) *in situ* measurements. Other temporal statistics included: bias, Nash-Sutcliffe coefficients (NS), and root mean square error (RMSE, in volumetric soil moisture). In terms of bias results are also evaluated based on whether the absolute bias is low (within 10%) or high (greater than 10%), which strongly impacts the other objective metrics. Each of these metrics has their own utility as discussed in the paper below.

3.4 Calibration of T_{opt}

Albergel et al. (2008) noted no significant correlation between soil properties and the optimal timescale of soil moisture variation (T_{Opt}). Therefore, they constrained this parameter by optimizing T based on the NS metric, an approach also applied by Ford et al. (2014). However, Albergel et al. (2008) also noted a weak relationship between T with climate. Specifically, a linkage between increased temperatures and, hence, soil evaporation (not transpiration). A lower T_{Opt} was representative of a faster response of SWI present in areas with a higher evaporational demand. This conjecture was consistent with a relationship developed by Qiu et al. (2014) using mean NDVI values at *in situ* sites.

In this study we used two approaches to determine T_{Opt}. The first method optimized T_{Opt} at a time in which the RMSE is minimized. This was essentially the same approach as finding a maximum NS value. RMSE was calculated between 1 to 68 days at a one-day increment. Sites that converged on the upper 68-day bound were rejected. Qiu et al. (2014) used a similar upper bound as a means of selecting SCAN sites for their study.

The second approach used the NDVI formulation from Qiu et al. (2014) to calculate T_{Opt}. This relationship is given as:

$$T_{Opt} = [\, -75.263 \ X \ NDVI \,] + 68.171 \qquad (3)$$

3.5 *In Situ* Station Filtering and Data Denial Experiment

To ensure that the exponential filter was effective in producing a RZSM estimate, the ms (t_n) term was set based on surface (5 cm) *in situ* data instead of satellite data. Normally grid based satellite surface moisture estimates are used to drive the exponential filter. However, to establish a filter based on the quality of *in situ* data an initial estimate of RZSM is determined based on surface *in situ* data at the 5 cm level. Initial RZSM estimates with a NS value less than 0.50, which is a common threshold for defining a satisfactory match between *in situ* and simulated hydrologic

data (Moriasi *et al.*, 2007), were rejected. This filter removed many of the poor performing outliers (NS < -1.00) from consideration. Table 2 describes the issues with the remaining poor performing outliers that lingered after this *in situ* based filtering approach.

Use of surface (5 cm) *in situ* data also supported a data denial experiment that gauged how the filter's performance was impacted by gaps in the ms (t_n) time series. This experiment focused on the SCAN network during era 3 (2005-2008; Table 1). Time series were altered to include only data at 2, 5, 8, and 11-day intervals. This experiment was based on the 32 out of 42 sites that had *in situ* based NS in excess of 0.50; i.e. the sites that survived this filtering process. Both surface (5 cm) *in situ* and satellite (AMSR-E) were used in this experiment.

3.6 Spurious Data Filtering

Before calculation of SWI values for all four satellite products at each *in situ* station, a series of filters were applied to remove any spurious results following the quality control guidelines articulated by Dorigo et al. (2013). Surface temperature and precipitation data from co-located PRISM grid cells flagged problematic dates within the time series of each dataset. Satellite retrieval from days in which the minimum air temperature was less than 0 ^{o}C were removed from the SWI dataset. Satellite soil moisture retrieval were particularly fraught with difficulty under freezing conditions (Dorigo et al., 2011). Likewise precipitation can be problematic and days with greater than 1 mm / day were excised following the guidance of (Dorigo et al., 2013). Three additional flags related to the quality of the *in situ* data were applied. Days with values in excess of the porosity reported by the ISMN were expunged from the rescaled SWI dataset. Likewise, days that recorded the same value (plateaus) or zero were deemed spurious and removed. The final filtered rescaled SWI dataset consisted of less than 100 days this dataset was rejected following the guidance of Dorigo et al. (2013). Finally, SWI based estimates in which NS < -1.00 were rejected as outliers. A detailed discuss of these outliers is given below.

4 Results

Figure 3 shows the results of the data denial experiment in which both *in situ* and satellite data (AMSR-E) was used at the surface. Note a baseline performance for *in situ* dataset has an average NS values close to 0.7, which was almost identical to results based on *in situ* surface soil moisture datasets in which every other day was withheld. Even in datasets with every four out of five dates withheld there was only a slight drop in performance. This result

underscored the ability of the exponential filter to effectively cope with datasets that have significant gaps. Average NS values fell to 0.5 only when over ninety percent of the surface soil moisture dataset was withheld and measurements from only every eleventh day were used. Data denial experiment using AMSR-E data to drive the filter yielded a similar drop-off in performance as the number of withheld days increased.

Figures 1 and 2 show lagged r-values between *in situ* surface (5 cm) and RZSM (20 to 30 cm) during the five eras. ARM sites clustered in Oklahoma and Kansas had higher lagged r-values during era 1 (Network Average r = 0.864) and a drop in this metric during eras 2 to 4 (Network Average r = 0.793 to 0.796). SCAN sites exhibited correlation coefficients that varied spatially. In general, better performances were noted from eastern (Network Average r = 0.751 to 0.872) and central sites (Network Average r = 0.812 to 0.874). Western sites had slightly lower r values (Network Average r = 0.699 to 0.770). Notable outliers were present for the stations in Montana during eras 4 and 5 (Fig. 2) that could account partly for the poorer performance noted during these eras. SNOTEL stations were concentrated in western CONUS and had consistently high correlation coefficients (Network Average r = 0.828 to 0.865). Finally the USCRN sites examined during era 5 (Table 1) generally had better r values in eastern and central CONUS (Network Average r = 0.846 to 0.882) as opposed to the west (Network Average r = 0.768).

The remainder of this section focuses on the results from the exponential filter driven by the four satellite products. The T_{Opt} and lagged r-values discussed are based on results that have a low absolute bias (± 10%). Note that the proportion of sites that recorded low bias varies between networks (data not shown). Most ARM stations were characterized by having low bias (76 to 100%) whereas SNOTEL sites had the lowest number of sites with a low bias (32 to 45%). SCAN (53 to 60%) and USCRN (60 to 66%) had an intermediate number of sites with a low bias. The subsequent results focused only on the low bias stations.

As might be expected, the T_{Opt} values from the NDVI approach had a much more limited range of values compared with T_{Opt} values derived using the optimization approach (Tables 3 to 6). From the ARM network average T_{Opt} based on the NDVI approach ranged from 32 to 36 days whereas optimization produced much greater variation (4 to 32 days; Table 3). At SCAN the NDVI approach yielded a broader range of average era T_{Opt} (28 to 46 days; Table 3). But again optimization produced more variable T_{Opt} values (9 to 39 days; Table 4). A similar pattern was noted at SNOTEL sites. The NDVI approach yielded higher network average era T_{Opt} values (42 to 45 days) versus the more variable and lower results from the optimization method (17 to 36 days; Table 5). Finally, USCRN sites

from era 5 (Table 1) exhibited a broad range of values for both approaches (NDVI = 30 to 55 days; Optimization = 9 to 28 days; Table 6).

Tables 3 to 6 show results from the direct correlation between *in situ* RZSM and SWI based estimates generated from the four satellite products. Network average values are excluded in this discussion if there were less than three measurements within an era for a network. Generally, but not always, the optimization approach yielded higher lagged r-values than NDVI. Interestingly, in the ARM network in 5 out of 14 instances the NDVI approach yielded network average r values that were greater than those obtained from the optimization method (Table 3). ARM sites from the central Great Plains had network average r values based on optimization that ranged from 0.450 to 0.707 across eras 1 to 4 (Table 1); whereas the NDVI approach yielded a lower and broader variation in r values (0.323 to 0.704; Table 3).

For SCAN sites comparisons were made only for eras 2 to 5 (Tables 1, 4). Era 1 was excluded in this comparison due to limited data availability during this period. Network average r-values based on optimization (0.458 to 0.720; Table 3) generally outperform those based on the NDVI approach (0.428 to 0.615; Table 4). Additionally, when examined from a geographic prospective, western CONUS sites had slightly higher r values based on optimization (0.477 to 0.823) than those from either the east (0.332 to 0.777) or central regions (0.492 to 0.717).

SNOTEL stations from the intermountain west showed the greatest variability. Some sites recorded r-values below 0, but there were also quite a few sites with high correlation coefficients (> 0.75). However, in general, network average r-values were lower in SNOTEL (optimization = 0.370 to 0.572; NVDI = 0.228 to 0.590) than at SCAN western sites (Table 5). Finally, the data from USCRN sites during era 5 (Table 1) had higher network average r-values in central sites versus western CONUS (Table 6).

NS values across the five eras were depicted in Figs. 4-6. Stations with low absolute bias (± 10%) consistently outperformed stations with high bias within all networks and during all eras. This was true for both the optimization and NDVI (data not shown) approaches to constraining T. Not surprisingly the optimization approach generally outperformed the NDVI method. Also, the four satellite products had quite consistent results and did not exhibit any clear temporal trends. All NS and RMSE network averages described below were based on the optimization approach to constraining T and had a low absolute bias. Figure 4 showed NS results from the ARM and USCRN networks. Network average NS values for ARM ranged from -0.1 to 0.3, similar to the results from the

USCRN network (0.2 to 0.3). Network average NS values from the SCAN and SNOTEL networks were shown in Figs. 5 and 6, which were slightly higher (0.1 to 0.5).

Figures 7-9 depicted RMSE values again across the five eras (Table 1). In many respects RMSE mirrors NS as a performance metric. Like NS stations, RMSE values with a low absolute bias outperformed those with high bias. However, the difference between low and high bias datasets was generally not as pronounced for the RMSE metric as it was for NS. But like with NS, RMSE results showed no discernable temporal trends. RMSE values from the ARM and USCRN networks were illustrated in Fig. 7. Network average RMSE values for ARM ranged from 0.02 to 0.04 and were significantly lower than values from the other networks examined in this study. USCRN network average RMSE values ranged from 0.04 to 0.05 (Fig. 7). Figure 8 illustrated results from the SCAN network and network average RMSE values were similar to USCRN sites (0.04 to 0.06). Finally, SNOTEL RMSE results (Fig. 9) were higher than all other networks (0.05 to 0.07).

5 Discussion and Conclusions

A long-standing goal of the soil remote sensing community has been to develop techniques that can observe changes in RZSM. Regrettably, the technology had not yet progressed to support a global RZSM product based only on remote sensing retrievals. The use of land surface models such as the community NOAH model (Chen et al., 1996), Global Land Data Assimilation System (GLDAS; Rodell et al., 2004), and European Centre for Medium-Range Weather Forecasts (ECMWF) Re-analysis products (Uppala et al., 2005; Massari et al., 2014) have been used to fill this gap in recent years. These platforms have become popular and provide an estimate of root zone soil moisture that has been applied to field scale studies (Albergel et al. 2012; Blankenship et al. 2016; Kedzior et al. 2016). In addition, another approach that has been suggested is based on thermal infrared based remote sensing *(e.g.* Hain et al., 2011).

Besides ease of use the exponential filter methodology is an attractive alternative because it leverages existing remotely sensed soil moisture platforms. As such, this approach is not hindered by the incipit assumptions built in to every modeling platform and relies purely on observational data. Given the potential utility of the exponential filter approach, a detailed analysis of the potential errors associated with the method is in order. There are four main sources of error. Two of these errors are associated with the SWI estimate and included: (1) the unsuitable of the exponential filter at a given site and (2) retrievals errors in the surface soil moisture dataset. The

other two errors are not related to the actual SWI estimate but instead are errors in the independent datasets that were applied to verify the SWI estimate at the scale of the 0.25^{o} satellite grid. These errors included: (3) issues with *in situ* datasets (Dorigo et al. 2011, 2013) and (4) non-representativeness of a point site when compared with the large (0.25^{o}) footprint of a surface soil moisture grid used to drive the filter (Crow et al. 2012). A significant quality control measure involved driving the filter with surface *in situ* instead of satellite soil moisture data. Stations that scored a NS < 0.5 based on this approach were rejected as not suitable. At these sites perhaps the fundamental assumption of the exponential filter method that there was hydrologic equilibrium between and the surface and root zone was violated. Therefore, the gross errors recorded at some sites cannot be ascribed to issues with the exponential filter and the data denial experiment demonstrated the robustness of this method at least in certain instances (Fig. 3).

Extending this approach we examined the quality of exponential filter results driven by surface *in situ* data against background conditions including soil texture, land cover, and climate zone (data not shown). In terms of soil texture, in situ sites with loamy textures has a general tendency to outperform (based on NS value) sand or clay dominated sites. This is not surprising given that the exponential filter generally works best when soil moisture is moderate (Ford et al 2014). Soil textures with a low available water capacity such as sand and clay are more likely to have extreme, both dry and wet, moisture contents. In terms of land cover the only consistent result is that in the SNOTEL network the more open rangeland settings exhibited slightly better NS values than forest dominated areas. However, this pattern was not observed at sites from the other networks. Finally, there is no clear trend in performance of the exponential filter as a function of climate zone.

Analysis of poor performing outliers (NS < -1.00) provided additional insights into how the exponential filter can fail at some sites (Table 2). Within the ARM network all outliers could be attributed to *in situ* data issues such as spikes, breaks, anomalous high values that exceed soil porosity, anomalous low values at zero, and extended plateaus (Dorigo et al. 2013). An example of such a clearly flawed *in situ* dataset is shown in Fig. 10 a. Within the SNOTEL network there was more of a mix in error type (Table 3). Besides *in situ* data issues, another significant source of error was the limited number of days in some of the final SWI datasets. Following the guidance of Dorigo et al. (2010) SWI datasets with less than 100 days were rejected. However, based on observations in this study, significant issues of representativeness were noted when there were less than 400 days (Fig. 10 b). The high altitude of many SNOTEL sites resulted in a longer freezing season during which a greater number of days were filtered out.

There were some sites with *in situ* data issues in the SCAN network (Table 2). However, many of the outliers also were caused by either SWI values that lacked the dynamic range of the *in situ* dataset (Fig. 10 c) or SWI values that had significant timing offsets compared with *in situ* RZSM observations (Fig. 10 d). These issues were the result of either site non-representativeness or errors in surface soil moisture retrievals. Finally, USCRN sites exhibited a similar mix of errors as noted in the SCAN network (Table 2).

A consistent result noted in this study was the impact of bias on other performance metrics. Consistently better results for all metrics were noted (Tables 3 to 6; Figs. 4-9) when there was a low absolute bias (within 10%) versus SWI datasets that had a high absolute bias (>10%). Additionally, this observation was observed for SWI values produced with both approaches to constrain T (minimization of RMSE and NDVI approach). The impact of bias on standard objective metrics was a focus of temporal stability analysis (Vachaud et al., 1985; Martinez-Fernandez and Ceballos, 2003). Sites with little variation in bias yielded more robust comparisons with remote sensing data (Starks et al., 2006); a result that was confirmed in this study across four distinct *in situ* soil moisture networks and satellite products.

Interestingly, the results observed in this study were more impacted by the *in situ* network than the surface satellite product used to drive the exponential filter. In terms of the NS metric, SCAN, SNOTEL, and USCRN outperformed ARM (Figs. 4-6). The NS metric seemed to have a greater utility in indentifying outliers than the RMSE metric. This was because it ranged from 1.00 to potentially $-\infty$, unlike RMSE, which ranged in this study from only 0 to 0.14.

Conversely, when considering the RMSE metric, ARM sites yielded superior scores compared with SCAN, SNOTEL, and USCRN (Figs. 7-9). Within the ARM network average RMSE was less than 0.04, which is the baseline value for accuracy designed for many satellite soil moisture missions (*e.g.* Kerr et al. 2001; Entekhabi et al., 2010). SCAN and USCRN were slightly above this guideline and were similar to RMSE values noted in previous *in situ*/satellite soil moisture comparisons (*e.g.* Brocca *et al.*, 2010; Jackson *et al.*, 2010, 2012; Al Bitar *et al.*, 2012). According to the RMSE metric SNOTEL sites performed the worst and was significantly above the 0.04 performance target.

Perhaps the most interesting result from this study was that the performance metrics in each *in situ* network did not vary over time. Given that almost two decades of data examined, this finding is particularly noteworthy. Therefore SWI estimates of RZSM produced by the exponential filter using CCI datasets can be leveraged for long-

term, perhaps even multi-decadal, climate studies (Manfreda et al., 2011). Another fruitful line of future research could compare exponential filter estimates of RZSM with those generated by land surface models. With the proliferation of space-based remote sensing platforms and the continued development of *in situ* monitoring networks the duration of RZSM time series will only grow. As such, the approaches outlined in this work can provide the cornerstone to support future assessments of long-term trends in RZSM, which is an essential climate variable.

Acknowledgements. We acknowledge the support of the NASA Climate Indicator and Data Products for Future National Climate Assessments program through award # NNX16AH30G. The assistance of Robert Parinussa (University of New South Wales), Arturo Diaz (Texas A&M International University), and Luis Carrasco Garza (Texas A&M International University) is greatly appreciated.

Reference

Albergel, C., Ruediger, C., Pellarin, T., *et al,*: From near-surface to root-zone soil moisture using an exponential filter: an assessment of the method based on in-situ observations and model simulations, Hydrology and Earth System Sciences, 12, 1323-1337, 2008.

Albergel, C., de Rosnay, P., Balsamo, G., Isaksen, L., and Munoz-Sabater, J.: Soil moisture analyses at ECMWF: evaluation using global-based in situ observations, Remote Sensing of Environment, 118, 215-226, 2012.

Al Bitar, A., Leroux, D., Kerr, Y. H., *et al.,* Evaluation of SMOS soil moisture products over Continental US using the SCAN/SNOTEL Network, IEEE Transactions on Geoscience and Remote Sensing, 50, 1572-1586, 2012.

Bartalis, Z., Wagner, W., Naeimi, V., Hasenauer, S., Scipai, K., Bonekmap, H., Figa, J., and Anderson, C.: Initial soil moisture retrievals from the METOP-A Advanced Scatterometer (ASCAT), Hydrology and Land Surface Studies, 34, L02401, 2007.

Bell, J.E., Palecki, M.A., Baker. C.B., Collins, W.G., Lawrimore, J.H., Leeper, R.D., Hall, M.E., Kochendorfer, J., Meyers, T.P., Wilson, T., and Diamond, H.J.: U.S. Climate Reference Network soil moisture and temperature observations, Journal of Hydrometeorology, 14, 977-988, 2013.

Blankenship, C.B., Case J.L., Zavodsky, B.T., Crosson, W.L.: Assimilation of SMOS retrievals in the Land Information System, IEEE Transactions on Geoscience and Remote Sensing, 54, 6320-6332, 2016.

Bolten, J.D., Crow, W.T., Zhan, X., *et al.*.: Evaluating the utility of remotely sensed soil moisture retrievals for operational agricultural drought monitoring, IEEE Journal of Selected Topics in Applied Earth Observations and Remote Sensing, 3, 57-66, 2010.

Bolten, J.D., and Crow, W.T.: Improved prediction of quasi-global vegetation conditions using remotely-sensed surface soil moisture, Geophysical Research Letters, 39, L19406, doi:10.1029/2012GL053470, 2012.

Brocca, L., Melone, F., Moramarco, T., Wagner, W., Naeimi, V., Bartalis, Z, and Hasenauer, S.: Improving runoff

prediction through the assimilation of the ASCAT soil moisture product, Hydrol. Earth Syst. Sci, 14, 1881-1893, 2010.

Brocca, L., Morbidelli, R., Melone, F., and Moramarco, T.: Soil moisture spatial variability in experimental areas of central italy, Journal of Hydrology, 333, 356-373, 2007.

Chen, F., Mitchell, K., Schakke, J., Xue, Y., Pan, H., Koren, V., Duan, Y., Ek, M., and Betts, A.: Modeling of land-surface evaporation by four schemes and comparison with FIFE Observations, Journal of Geophysical Research, 101, 7251-7268, 1996.

Daly C., Neilson, R.P., Phillips, D.L.: A statistical-topographic model for mapping climatological precipitation over mountainous terrain, Journal of Applied Meteorology, 33, 140-158, 1994.

Didan, K: 2015, MODIS13Q1 MODIS/Terra Vegetation Indices 16-Day L3 Global 250 m SIN Grid V006, NASA EOSDIS, Land Processes DAAC, https://doi.org/10.5067/MODIS/MOD13Q1.006

Dorigo, W.A., Scipal, K., Parinussa, R.M., Liu, Y.Y., Wagner, W., de Jeu, R.A.M., and Naeimi, V.: Error characterisation of global active and passive microwave soil moisture datasets. Hydrology and Earth System Sciences 14, 2605-2616, doi:10.5194/hess-14-2605-2010, 2010.

Dorigo, W.A., Wagner, W., and Hohensinn, R.: The International Soil Moisture Network: a data hosting facility for global in situ soil moisture measurements, Hydrology and Earth System Sciences, 15, 425-436, 2011.

Dorigo, W. A., Xavier, A., Vreugdenhill, M, *et al*.: Global automated quality control of in situ soil moisture data from the International Soil Moisture Network, Vadose Zone Journal. 2013.

Entekhabi, D, et al.: The Soil Moisture Active Passive (SMAP) mission. Proceedings of IEEE, 98, 704-716. 2010.

Ford, T.W., Harris, E., and Quiring, S.M.: Estimating root zone soil moisture using near- surface observations from SMOS, Hydrol. Earth Syst. Sci, 18, 139-154, 2014.

Hain, C.R., Crow, W.T, Mecikalski, J.R. Anderson, M.C., and Holmes, T.: An intercomparison of available soil moisture estimates from thermal-infrared and passive microwave remote sensing, Journal of Geophysical Research-Atmospheres, 166, 2011JD015633, 2011.

Hutchinson, J.M.S.: Estimating near-surface soil moisture using active microwave satellite imagery and optical sensor inputs, Transactions of the ASAE, 46, 225-236, 2003.

Jackson, T.J, Le Vine, D.M., Hsu, A.Y., Oldak, A., Starks, P.J., Swift, C.T., Isham, J.D., and Haken, M., Soil moisture mapping at regional scales using microwave radiometry: The Southern Great Plains Hydrological Experiment, IEEE Transaction in Geoscience and Remote Sensing, 37. 2136-2151, 1999

Jackson, T.J., Hsu, A.Y., O'Neill, P.E.: Surface soil moisture retrieval and mapping using high- frequency microwave satellite observations in the Southern Great Plains, Journal of Hydrometeorology, 3, 688-699, 2002.

Jackson, T.J., Cosh, M.H., Bindlish, R. Starks, P.J., Bosch, D.D., Seyfried, M., Goodrich D.C., Moran, M.S., and Du, J.: Validation of Advanced Microwave Scanning Radiometer Soil Moisture Products, IEEE Transaction in Geoscience and Remote Sensing, 48, 4256-4272, 2010.

Jackson, T.J., Bindlish, R., Cosh, M.H., et al.: Validation of Soil Moisture and Ocean Salinity (SMOS) Soil Moisture Over Watershed Networks in the U.S., IEEE Transactions of Geoscience and Remote Sensing, 50,

448 1530-1543, 2012.
449 Kedzior, M., and Zawadski, J.: Comparative study of soil moisture from SMOS satellite mission, GLDAS database,
450 and cosmic ray-neutrons measurements at COSMOS in Eastern Poland, Geoderma, 283, 21-31, 2010.
451 Klute, A.: Water retention: Laboratory methods. Methods of Soil Analysis: Part 1, Physical and Minerological
452 Methods, A. Klute, Ed., American Society of Agronomy and Soil Science Society of America, 635–662, 1986.
453 Kerr, Y.H., Waldteufel, P., Wigneron, J.P., Maerinuzzi, J.M., Font, J., and Berger, M.: Soil moisture retrieval from
454 space: The Soil Moisture and Ocean Salinity (SMOS) mission, IEEE Transactions of Geoscience and Remote
455 Sensing, 39, 1729-1735, 2001.
456 Kumar, S.V., Reichle, R.H., Koster, R.D., Crow, W.T., and Peters-Lidard, C.D.: Role of subsurface physics in the
457 assimilation of surface soil moisture observations, Journal of Hydrometeorology, 10, 1534-1547, 2009.
458 Lakshmi, V. Wood, E.F., and Choudhury, B.J.: Investigation of effect of heterogeneities in vegetation and rainfall
459 on simulated SSM/I brightness tempeatures, Journal of Applied Meteorology, 36, 1309-1328, 1997.
460 Lettenmaier, D.P., Alsdorf, D., Dozier, J., Huffman, G.J., Pan, M., and Wood, E.F.: Inroads of remote sensing into
461 hydrologic science during the WRR era. Water Resources Research, 51, 7309-7342, 2015.
462 Liu, Y. Y., and Coauthors: Trend-preserving blending of passive and active microwave soil moisture retrievals,
463 Remote Sensing of Environment, 123, 280-297, 2012.
464 Manfreda, S., Lacava, T., Onorati, B., Pergola, N, Di Leo, M., Margiotta, M.R., and Tramutoli, V.: On the use of
465 AMSU-based products for the description of soil water content at basin scale, Hydrol. Earth Syst. Sci, 15, 2839-
466 2852, 2011.
467 Manfreda, S, Brocca, L., Moramacro, T., Melone, F., Sheffield, J.: A physically based approach for the estimation
468 of root-zone soil moisture from surface measurements, Hydrol. Earth Syst. Sci, 18, 1199-1212, 2014.
469 Martinez-Fernandez, J., and Ceballos, A.: Mean soil moisture estimation using temporal stability Analysis, Journal
470 of Hydrology, 312, 28-38, 2005.
471 Massari, C., Brocca, L., Barbetta, S., Papathanasiou, C., Mimikou, M., & Moramarco, T.: Using globally available
472 soil moisture indicators for flood modeling in Mediterranean catchments, Hydrol. Earth Syst. Sci, 18(2), 839–853,
473 2014.
474 McCabe, M.F., Gao, H, and Wood, E.F.: Evaluation of AMSR-E-derived soil moisture retrievals using ground-
475 based and PSR airborne data using SMEX02, Journal of Hydrometeorology, 6, 864-877, 2005.
476 Moriasi, D. N., Arnold, J. G., Van Liew, M. W., Bingner, R. L., Harmel, R. D., and Veith, T. L.: Model evaluation
477 guidelines for systematic quantification of accuracy in watershed simulations, Transactions of the ASABE, 50,
478 885-900, 2007.
479 Njoku, E.G., Jackson, T.J., Lakshmi, V., Chan, T.K., and Nghiem, S.V.: Soil moisture retrieval from AMSR-E,
480 IEEE Transactions of Geoscience and Remote Sensing, 41, 215-229, 2003.
481 Owe M., De Jeu, R.A.M., and Holmes, T.R.H.: Multisensor historical climatology of satellite-derived global land
482 surface moisture, Journal of Geophysical Research-Earth Surface, vol. 113. 2008.
483 Peterson, A.M., Helgason, W.D., Ireson, A.M.: Estimating field-scale root zone soil moisture using the cosmic-ray

neutron probe, Hydrol. Earth Syst. Sci, 20, 1373-1385, 2016.

Qiu, J. Crow, W.T., Nearing, G.S., Mo, X., Liu, S.: The impact of vertical measurement depth on the information content of soil moisture time series data, Geophysical Research Letters, 41, 4997-5004, 2014.

Reece, C. F.: Evaluation of a line heat dissipation sensor for measuring soil matric potential. Soil Science Society of America Journal, 60, 1022–1028, 1996.

Reichle, R. De Lannoy, G., Koster, R., Crow, W., and Kimball, J.: SMAP L4 9 km EASE-Grid Surface and Root Zone Soil Moisture Geophysical Data, Version 2, NASA National Snow and Ice Data Center, 2016.

Rodell, M., Houser, P.R., Jambor, U., Gottschalck, J., Mitchell, K., Meng, C-J., Arsenault, K., Cosgrove, R., Radakovich, J., Bosilovich, M., Entin, J.K., Walker, L.P., Lohmann, D., and Toll, D.: The global data land surface assimilation system, Bulletin of American Meteorological Society, 85, 381-394, 2004.

Schaefer, G. L., Cosh, M. H., and Jackson, T. J.: The USDA Natural Resources Conservation Service Soil Climate Analysis Network (SCAN), Journal of Atmospheric and Oceanic Technology, 24, 2073–2077. 2007.

Seyfried, M. S., Grant, L. E., Du, E., and Humes, K.: Dielectric loss and calibration of the Hydra Probe soil water sensor. Vadose Zone Journal, 4, 1070–1079, 2005.

Starks, P.J., Heathman, G.C., Jackson, T.J., Cosh, M.H.: Temporal stability of soil moisture profile, Journal of Hydrology, 324, 400-411, 2006.

Uppala SM, et al.: The ERA-40 re-analysis, Quarterly Journal of the Royal Meteorological Society, 131, 2961-3012, 2005.

Vachaud, G., DeSilnas, A.P., Balabanis, P., Vauclin, M., Temporal stability of spatially measured soil water probability density function, Journal of Soil Science Society of America, 49, 822-828, 1985.

Wagner, W; Lemoine, G; Rott, H., 1999: A method for estimating soil moisture from ERS scatterometer and soil data, Remote Sensing of the Environment, 70: 191-207.

Wagner W., K. Scipal, C. Pathe, D. Gerten, W. Lucht, and B. Rudolf, 2003: Evaluation of the agreement between the first global remotely sensed soil moisture data with model and precipitation data, Journal of Geophysical Research-Atmospheres, vol. 108, .

Wentz, F.J, Meissner, T, Gentemann, C., Hilburn, K.A., Scott, J.: Remote sensing systems GCOM-W1 AMSR2 Environmental Suite on 0.25 deg grid, Remote Sensing Systems, Santa Rosa, Calfornia, U.S.A., 2014.

Western, A. W., Zhou, S. L., Grayson, R. B., McMahon, T. A., Bloschl, G., and Wilson, D. J.: Spatial correlation of soil moisture in small catchments and its relationship to dominant spatial hydrological processes, Journal Of Hydrology, 286, 113-134, 2004.

Wilson, D. J., Western, A. W., and Grayson, R. B.: Identifying and quantifying sources of variability in temporal and spatial soil moisture observations, Water Resources Research, 40, W02507, 2004.

TABLES

Table 1. Observation eras from 1997 to 2014.

Era	Description	Time Range
1	Pre-AMSR-E	November 27 1997 to June 18 2002
2	Early AMSR-E	June 19 2002 to June 30 2005
3	Middle AMSR-E	July 1 2005 to June 30 2008
4	Late AMSR-E	July 1 2008 to October 3 2011
5	Post-AMSR-E	October 4 2011 to December 31, 2014

519

520 Table 2. Number of poor performing (NS < 1.00) outliers for all four satellite products.

521 RMSE Optimization

	ARM	SCAN	SNOTEL	USCRN
In situ Data	17	3	15	1
Insufficient SWI	0	1	14	0
Lack of Range	0	11	0	3
Timing Issues	0	0	9	0

522

523 NDVI Approach

	ARM	SCAN	SNOTEL	USCRN
In situ Data	22	16	32	5
Insufficient SWI	0	3	44	0
Lack of Range	0	17	15	8
Timing Issues	0	6	5	3

524

525

Table 3. Average lagged r-values and T_{Opt} between SWI based and *in situ* soil moisture at the 25 cm depth for the ARM network. Standard derivation is indicated in parentheses. The n value represents the number of observations.

Optimization Approach – Low Bias

	AMSR-E			CCI-Combined			CCI-Passive			CCI-Active	
Era	**n**	**r value**	**T_{opt}**	**n**	**r value**	**T_{opt}**	**n**	**r value**	**T_{opt}**	**n**	**r value**	**T_{opt}**
1	---	--------	----	14	0.471 (0.249)	30 (19)	4	0.614 (0.131)	25 (29)	9	0.450 (0.193)	26 (13)
2	9	0.587 (0.080)	4 (1)	10	0.491 (0.136)	9 (4)	10	0.554 (0.103)	7 (6)	11	0.493 (0.153)	17 (7)
3	12	0.589 (0.148)	7 (3)	12	0.520 (0.156)	12 (10)	12	0.615 (0.165)	8 (4)	12	0.460 (0.165)	13 (10)
4	4	0.666 (0.053)	32 (10)	3	0.707 (0.081)	10 (4)	2	0.649 (0.011)	12 (1)	1	0.823	5

NDVI Approach– Low Bias

	AMSR-E			CCI-Combined			CCI-Passive			CCI-Active	
Era	**n**	**r value**	**T_{opt}**	**n**	**r value**	**T_{opt}**	**n**	**r value**	**T_{opt}**	**n**	**r value**	**T_{opt}**
1		--------	----	17	0.439 (0.241)	36 (3)	9	0.480 (0.171)	36 (2)	12	0.414 (0.172)	36 (4)
2	7	0.622 (0.156)	35 (3)	11	0.567 (0.172)	34 (4)	9	0.642 (0.132)	34 (4)	13	0.484 (0.154)	32 (3)
3	13	0.559 (0.204)	34 (2)	12	0.437 (0.179)	35 (3)	10	0.645 (0.137)	34 (3)	12	0.341 (0.197)	34 (3)
4	5	0.666 (0.053)	32 (6)	3	0.704 (0.004)	34 (2)	3	0.665 (0.542)	34 (2)	7	0.323 (0.184)	32 (3)

Table 4. Average lagged r-values and T_{Opt} between SWI based on optimization and *in situ* soil moisture at the 20.32 cm depth for the SCAN network (Figures 1 and 2). Standard derivation is indicated in parentheses. The n value represents the number of observations.

Optimization Approach – Low Bias

	AMSR-E			CCI-Combined			CCI-Passive			CCI-Active	
Era	**n**	**r value**	**T_{opt}**	**n**	**r value**	**T_{opt}**	**n**	**r value**	**T_{opt}**	**n**	**r value**	**T_{opt}**
1	---	--------	----	1	0.817	19	1	0.691	1	3	0.458 (0.323)	22 (10)
2	4	0.691 (0.157)	39 (19)	7	0.598 (0.157)	27 (16)	2	0.661 (0.007)	16 (9)	7	0.519 (0.147)	15 (6)
3	17	0.596 (0.129)	10 (7)	19	0.556 (0.164)	14 (13)	16	0.556 (0.184)	9 (5)	17	0.521 (0.140)	17 (17)
4	14	0.697 (0.096)	15 (14)	16	0.698 (0.155)	19 (15)	10	0.720 (0.176)	15 (12)	16	0.642 (0.226)	17 (16)
5	---	--------	----	17	0.572 (0.183)	16 (15)	11	0.472 (0.192)	21 (14)	15	0.589 (0.195)	14 (14)

NDVI Approach– Low Bias

	AMSR-E			CCI-Combined			CCI-Passive			CCI-Active	
Era	**n**	**r value**	**T_{opt}**	**n**	**r value**	**T_{opt}**	**n**	**r value**	**T_{opt}**	**n**	**r value**	**T_{opt}**
1	---	--------	----	2	0.678 (0.199)	32 (6)	2	0.747 (0.096)	49	4	0.463 (0.282)	40 (10)
2	6	0.554 (0.198)	34 (16)	7	0.541 (0.179)	30 (12)	1	0.330	20	10	0.505 (0.171)	28 (7)
3	14	0.596 (0.111)	31 (10)	15	0.480 (0.193)	34 (11)	15	0.613 (0.095)	36 (11)	15	0.471 (0.187)	31 (10)
4	16	0.573 (0.242)	37 (15)	20	0.585 (0.223)	39 (15)	14	0.615 (0.238)	39 (15)	20	0.608 (0.226)	40 (15)
5	---	--------	----	19	0.518 (0.220)	39 (13)	15	0.428 (0.238)	46 (11)	26	0.469 (0.237)	41 (13)

549 Table 5. Average lagged r-values and T_{Opt} between SWI based on optimization and *in situ* soil
550 moisture at the 20.32 cm depth for the SNOTEL network. Standard derivation is indicated in
551 parentheses. The n value represents the number of observations.
552
553 Optimization Approach – Low Bias
554

	AMSR-E			CCI-Combined			CCI-Passive			CCI-Active	
Era	**n**	**r value**	**T_{opt}**	**n**	**r value**	**T_{opt}**	**n**	**r value**	**T_{opt}**	**n**	**r value**	**T_{opt}**
2	5	0.572 (0.311)	17 (15)	2	0.600 (0.034)	10 (1)	2	0.750 (0.054)	14 (7)	3	0.509 (0.156)	36 (13)
3	39	0.463 (0.264)	20 (15)	17	0.513 (0.290)	27 (18)	30	0.461 (0.293)	25 (20)	30	0.370 (0.317)	29 (11)
4	63	0.508 (0.299)	18 (14)	32	0.491 (0.353)	20 (16)	55	0.522 (0.302)	18 (11)	32	0.522 (0.379)	22 (18)
5	---	--------	----	5	0.527 (0.189)	25 (13)	12	0.412 (0.252)	26 (17)	8	0.534 (0.319)	27 (21)

555
556 NDVI Approach– Low Bias
557

	AMSR-E			CCI-Combined			CCI-Passive			CCI-Active	
Era	**n**	**r value**	**T_{opt}**	**n**	**r value**	**T_{opt}**	**n**	**r value**	**T_{opt}**	**n**	**r value**	**T_{opt}**
2	2	0.678 (0.197)	44 (13)	1	0.438	49	4	0.584 (0.102)	45 (8)	4	0.444 (0.362)	44 (7)
3	44	0.367 (0.374)	44 (6)	28	0.313 (0.395)	44 (7)	43	0.334 (0.386)	44 (6)	45	0.327 (0.337)	44 (5)
4	71	0.425 (0.367)	43 (6)	33	0.385 (0.491)	43 (7)	61	0.451 (0.341)	44 (7)	41	0.228 (0.529)	44 (6)
5	---	--------	----	11	0.425 (0.216)	44 (7)	9	0.357 (0.318)	43 (5)	10	0.590 (0.268)	42 (6)

558
559
560

Table 6. Average lagged r-values T_{Opt} between SWI based on optimization and *in situ* soil moisture at the 20 cm depth for the USCRN network during era 5. Standard derivation is indicated in parentheses. Sites are divided by region (east, central, west) as indicated on Figure 2. The n value represents the number of observations.

Optimization Approach – Low Bias

	CCI-Combined			**CCI-Passive**			**CCI-Active**		
Region	**n**	**r value**	**T_{opt}**	**n**	**r value**	**T_{opt}**	**n**	**r value**	**T_{opt}**
East	1	0.105	4	--	--------	----	1	0.486	15
Central	13	0.594 (0.185)	9 (8)	6	0.707 (0.086)	17 (19)	11	0.607 (0.126)	6 (3)
West	1	0.857	11	4	0.406 (0.125)	28 (21)	3	0.540 (0.389)	9 (1)

NDVI Approach– Low Bias

	CCI-Combined			**CCI-Passive**			**CCI-Active**		
Region	**n**	**r value**	**T_{opt}**	**n**	**r value**	**T_{opt}**	**n**	**r value**	**T_{opt}**
East	2	0.388 (0.122)	1	1	0.071	25	2	0.410 (0.133)	21
Central	12	0.521 (0.231)	30 (10)	7	0.605 (0.194)	35 (9)	7	0.534 (0.176)	25 (7)
West	3	0.209 (0.068)	36 (20)	4	0.342 (0.128)	45 (20)	3	0.087 (0.122)	55 (5)

Figure Captions

Figure 1. Locality map of examined *in situ* stations (ARM - X; SCAN - ∗; SNOTEL - +) with (**a**) era 1, (**b**) era 2, and (**c**) era 3. The gray area represents central CONUS whereas white indicates the eastern and western regions of CONUS.

Figure 2. Locality map of examined *in situ* stations (ARM - X; SCAN - ∗; SNOTEL - +) with (**a**) era 4 and (**b**) era 5. During era 5 (X) represents USCRN instead of ARM stations. The gray area represents central CONUS whereas white indicates the eastern and western regions of CONUS.

Figure 3. Box plot of data denial experiment from the SCAN network during era 3 (2005-2008). Results for day 1 represent baseline data for the exponential filter driven by surface soil moisture data (*in situ* data – stars; low absolute bias RMSE optimized AMSR-E – circles). Other time series were altered to include only data at 2, 5, 8, and 11-day intervals.

Figure 4. Box plots that depict the NS metric for the ARM (eras 1 to 4) and USCRN (era 5) networks. Results for high absolute bias RMSE optimized datasets are squares, low absolute bias RMSE optimized datasets are circles, and low absolute bias NVDI datasets are triangles.

Figure 5. Box plots depicting NS metric for the SCAN network. Symbols are as in Figure 4.

Figure 6. Box plots depicting NS metric for the SNOTEL network. Symbols are as in Figure 4.

Figure 7. Box plots depicting RMSE metric for the ARM (eras 1 to 4) and USCRN (era 5) networks. Symbols are as in Figure 4.

Figure 8. Box plots depicting RMSE metric for the SCAN network. Symbols are as in Figure 4.

Figure 9. Box plots depicting RMSE metric for the SNOTEL network. Symbols are as in Figure 4.

Figure 10. Selected time series associated with poorly performing (NS < 1.00) outliers with *in situ* data as solid gray and SWI estimates in dashed black. (**a**) Shows an example of problematic *in situ* data. (**b**) Is an example where there was insufficient SWI data. (**c**) Illustrates an SWI dataset that lacked the dynamic range present in the *in situ* data. (**d**) Depicts a discrepancy in timing between SWI and *in situ* datasets.

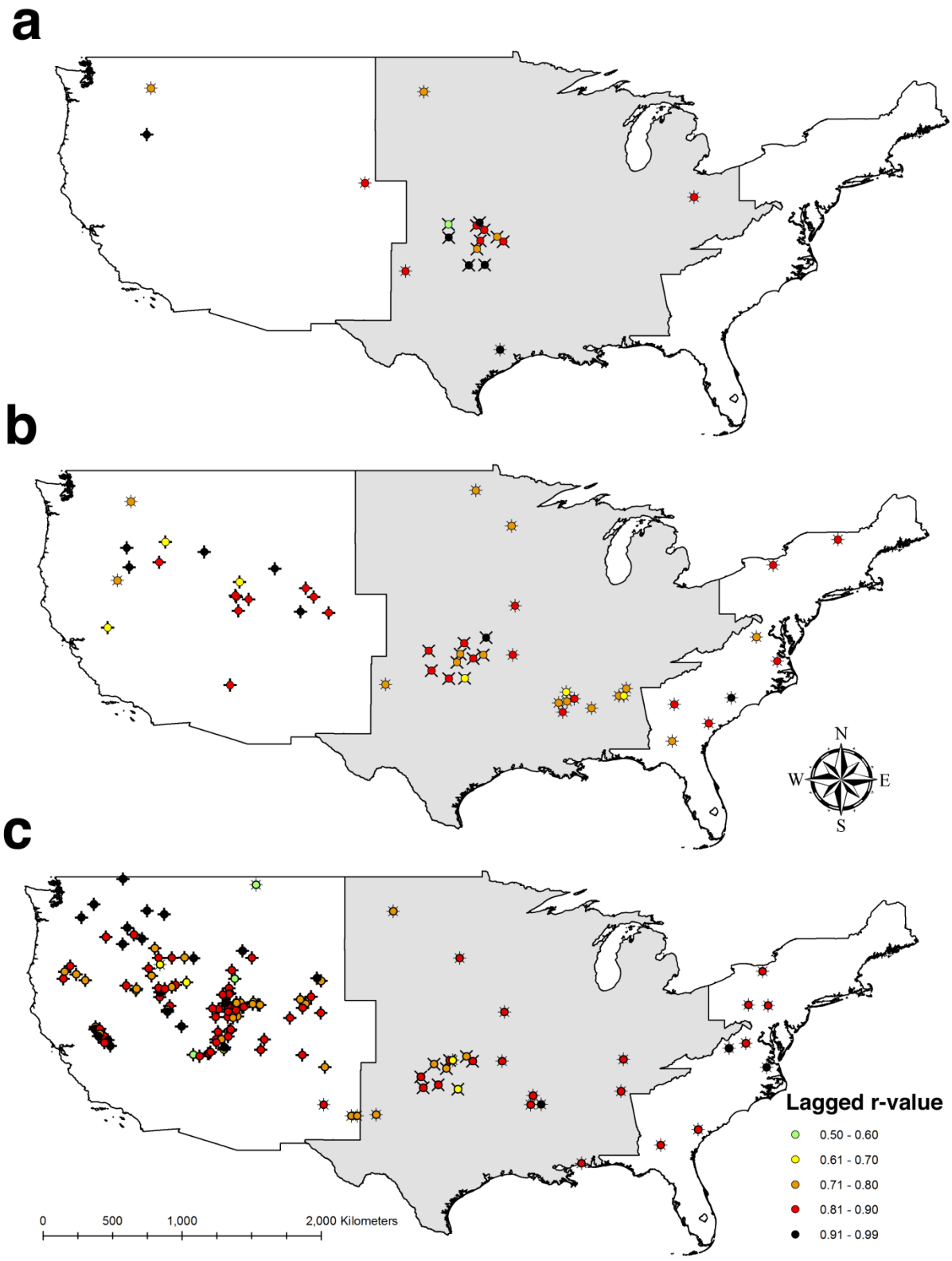
a
b
c
N
W
E
S
Lagged r-value
0.50 - 0.60
0.61 - 0.70
0.71 - 0.80
0.81 - 0.90
0.91 - 0.99
0
500
1,000
2,000 Kilometers

615

FIGURE 1 (Previous Page)

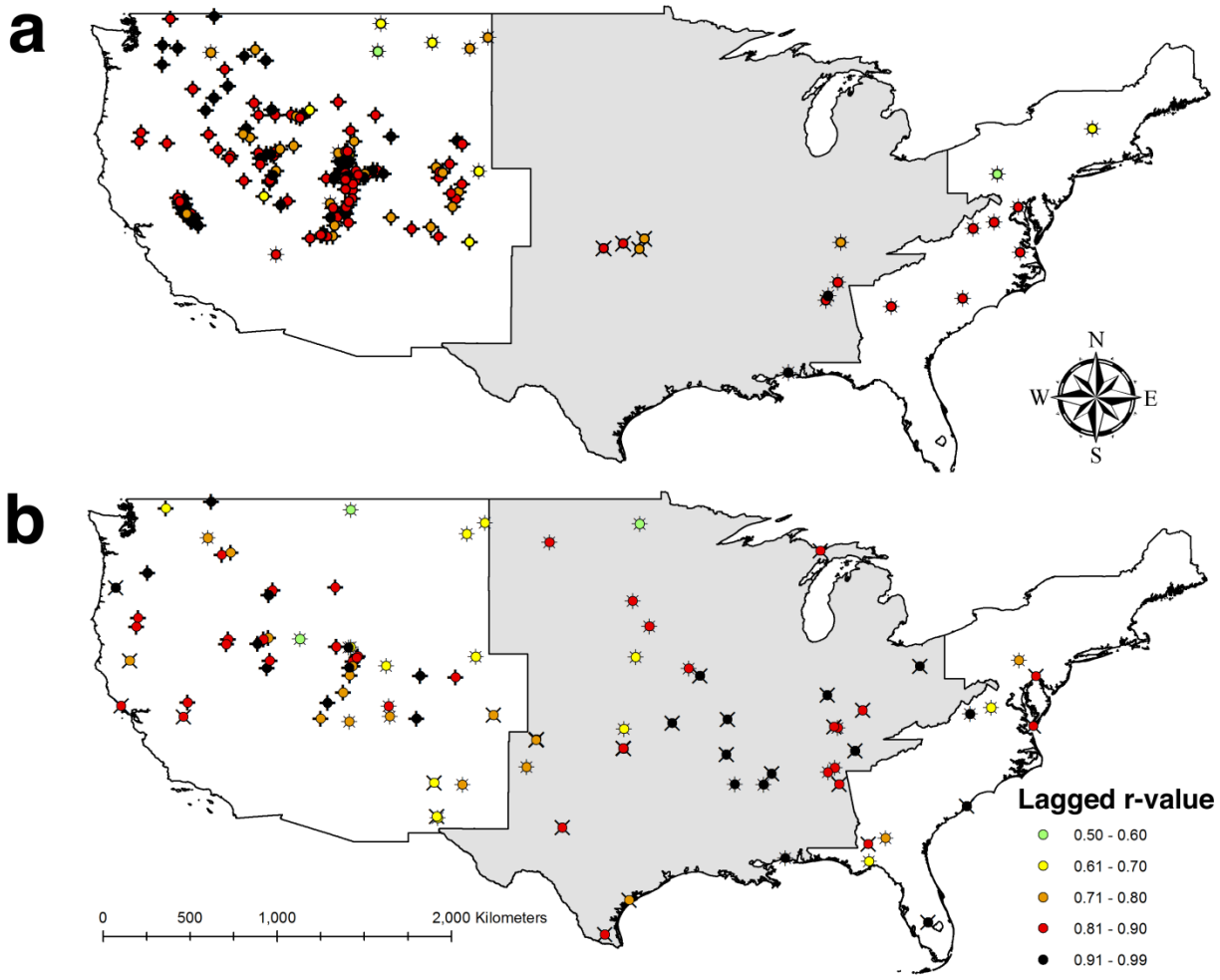

FIGURE 2

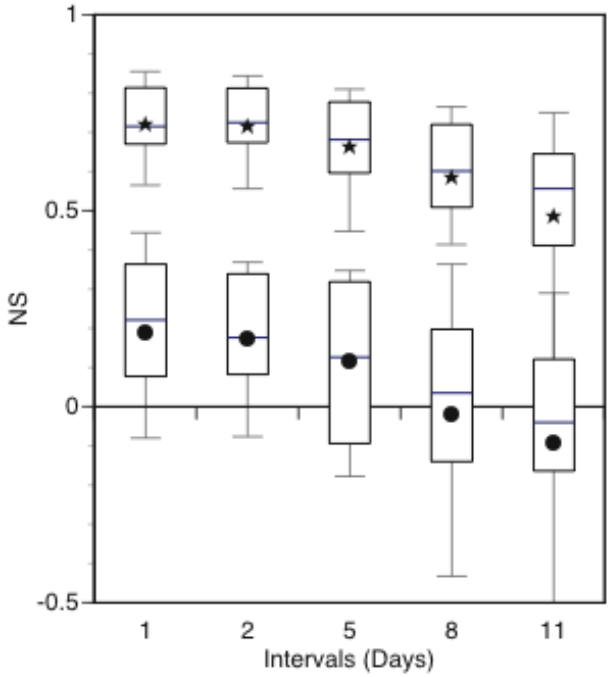

Figure 3

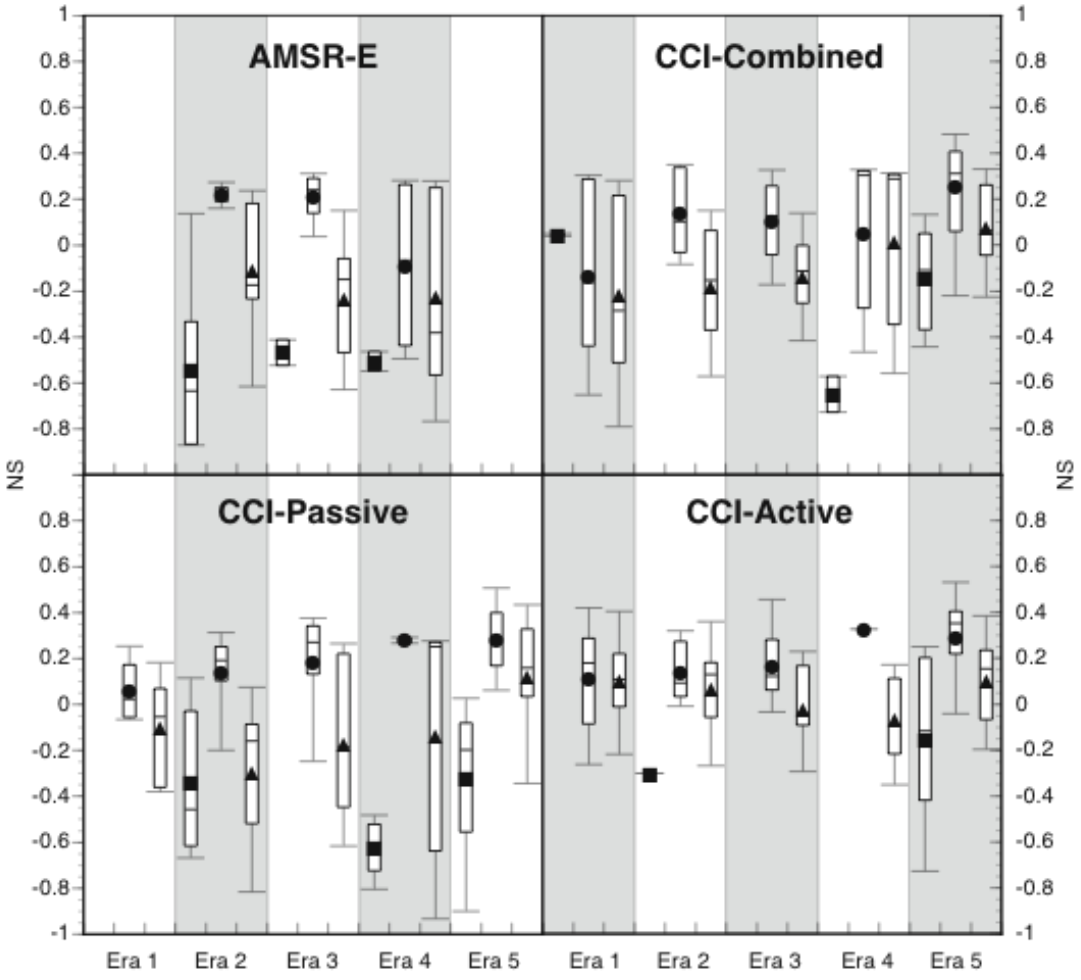
AMSR-E
CCI-Combined
CCI-Passive
CCI-Active
NS
NS
1
0.8
0.6
0.4
0.2
0
-0.2
-0.4
-0.6
-0.8
-1
Era 1
Era 2
Era 3
Era 4
Era 5

Figure 4

634

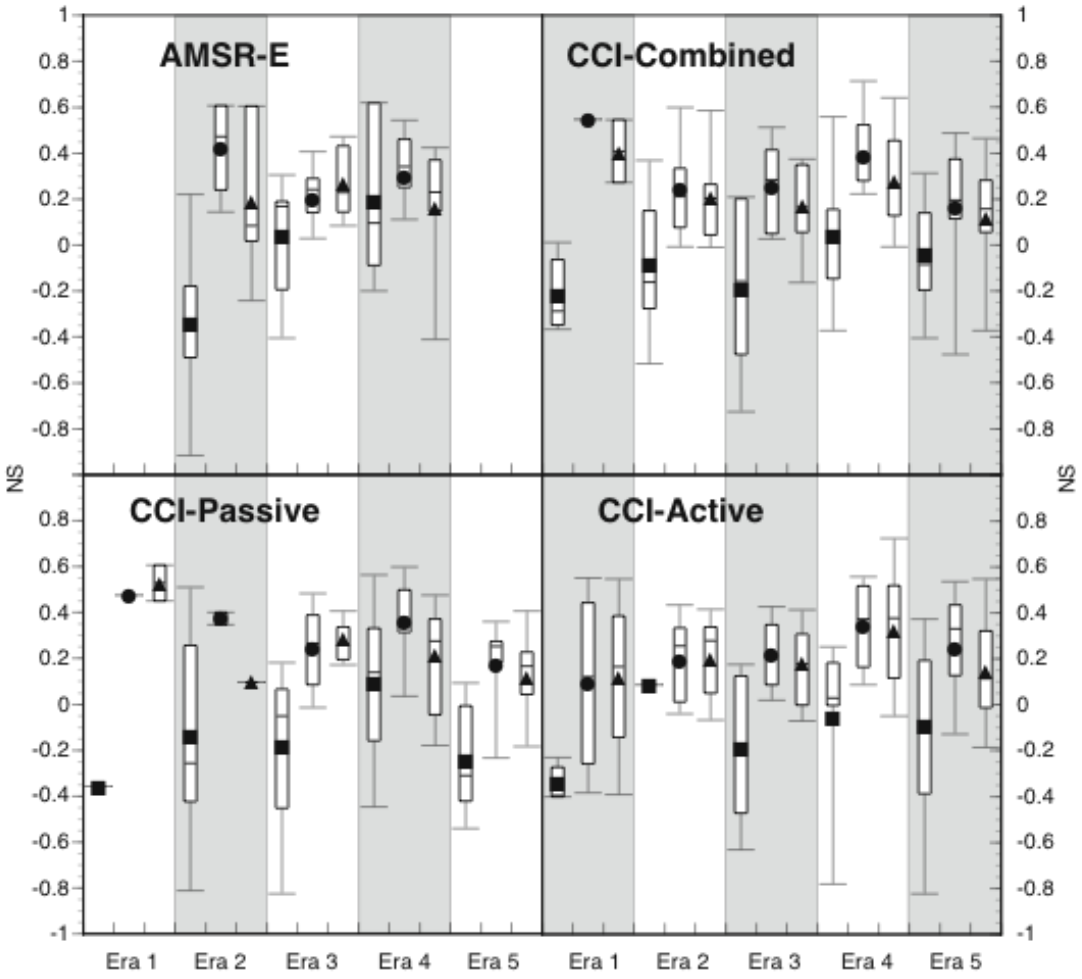
AMSR-E
CCI-Combined
CCI-Passive
CCI-Active
NS
NS
1
0.8
0.6
0.4
0.2
0
-0.2
-0.4
-0.6
-0.8
-1
Era 1
Era 2
Era 3
Era 4
Era 5

Figure 5

635

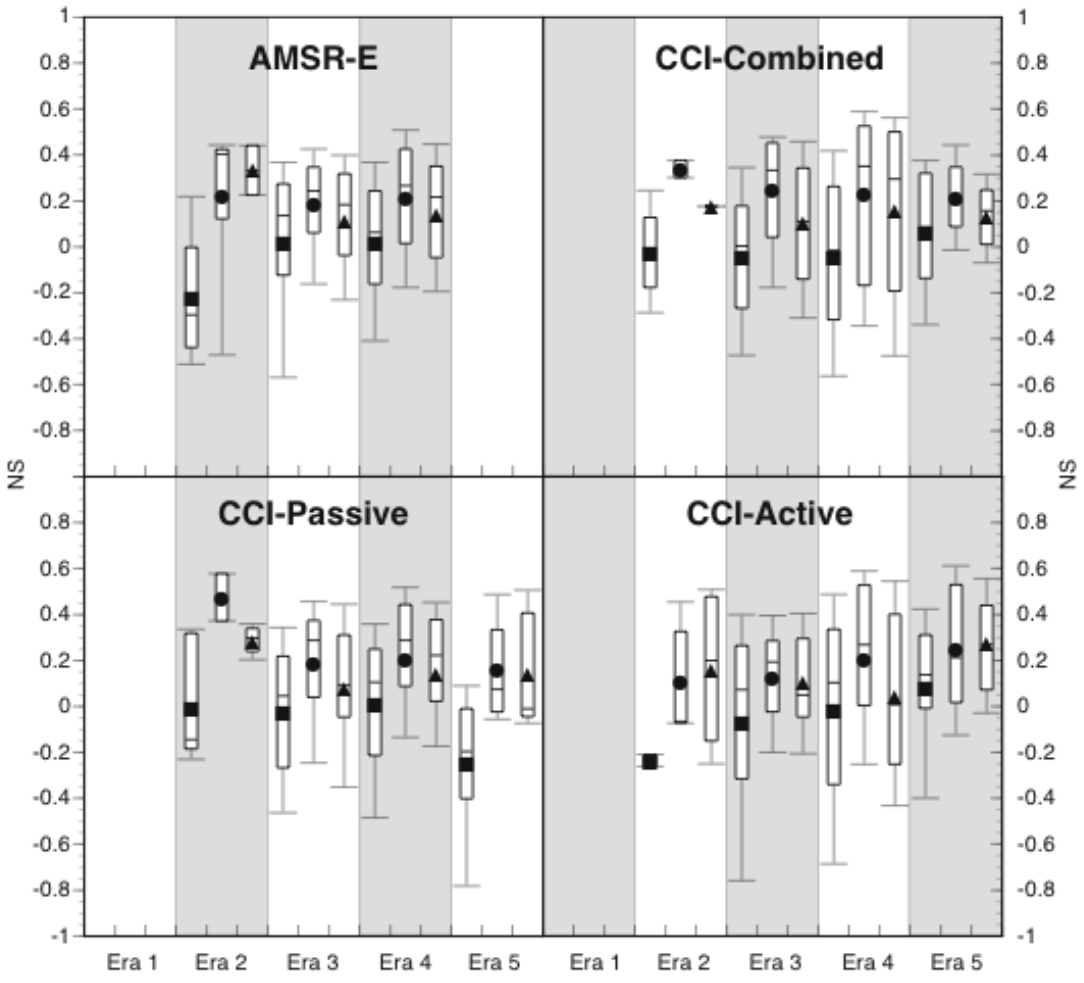
AMSR-E
CCI-Combined
CCI-Passive
CCI-Active
NS
NS
1
0.8
0.6
0.4
0.2
0
-0.2
-0.4
-0.6
-0.8
-1
Era 1
Era 2
Era 3
Era 4
Era 5

Figure 6

636

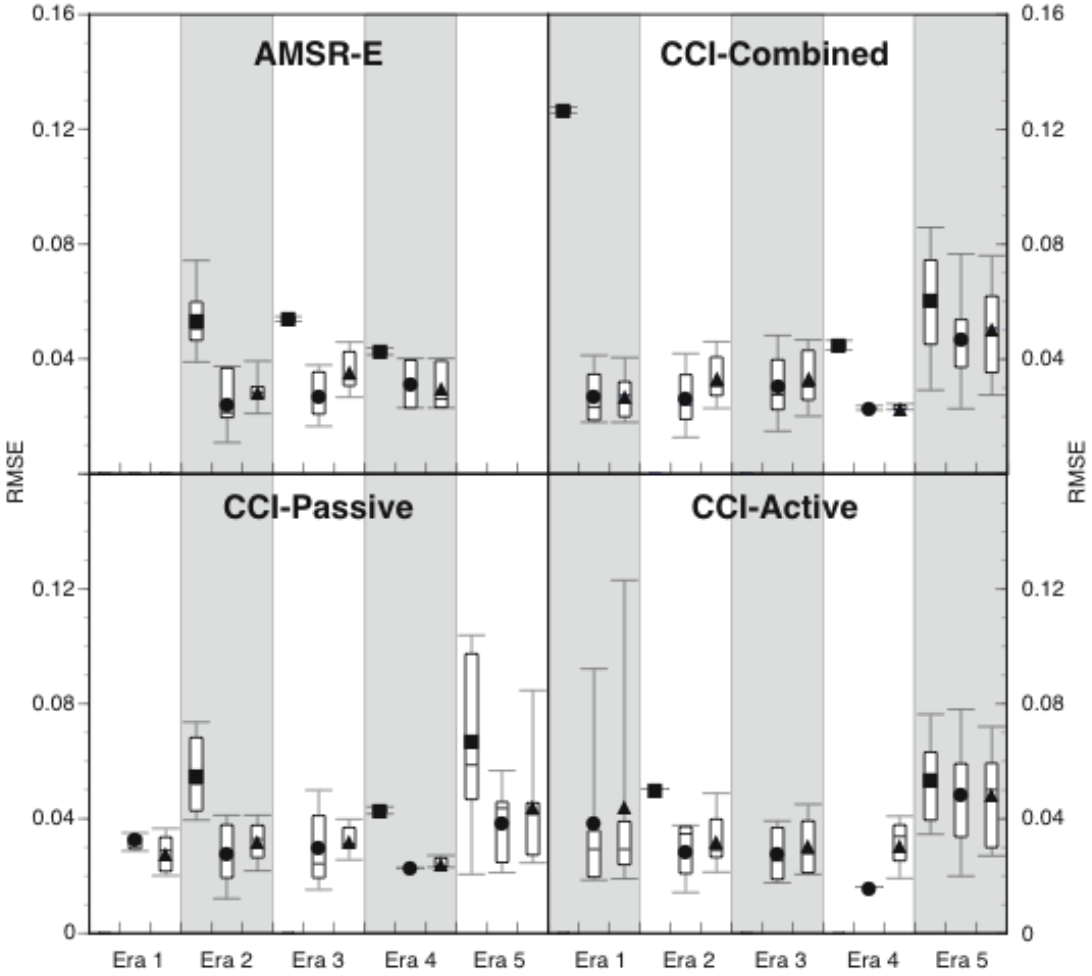
AMSR-E
CCI-Combined
CCI-Passive
CCI-Active
RMSE
RMSE
0.16
0.12
0.08
0.04
0
Era 1
Era 2
Era 3
Era 4
Era 5

Figure 7

637

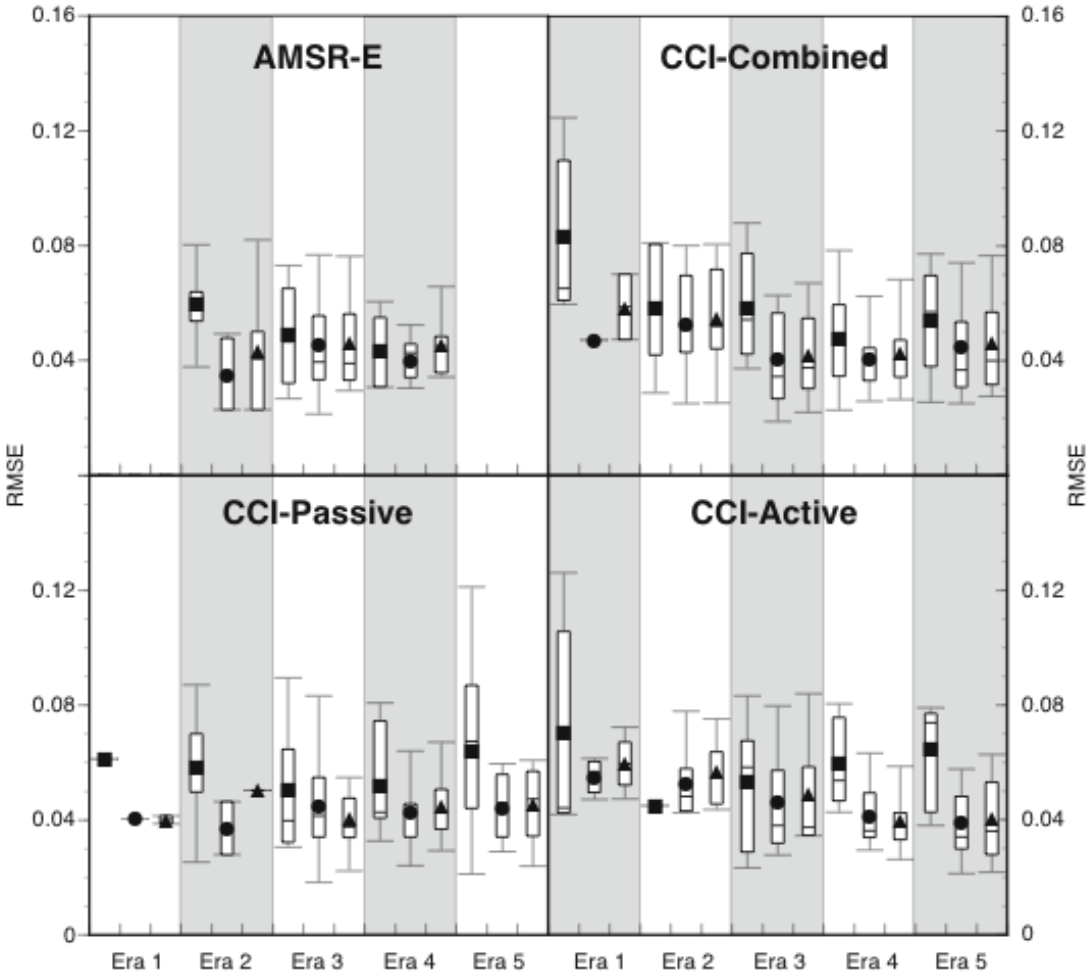
AMSR-E
CCI-Combined
CCI-Passive
CCI-Active
RMSE
RMSE
0.16
0.12
0.08
0.04
0
Era 1
Era 2
Era 3
Era 4
Era 5

Figure 8

638

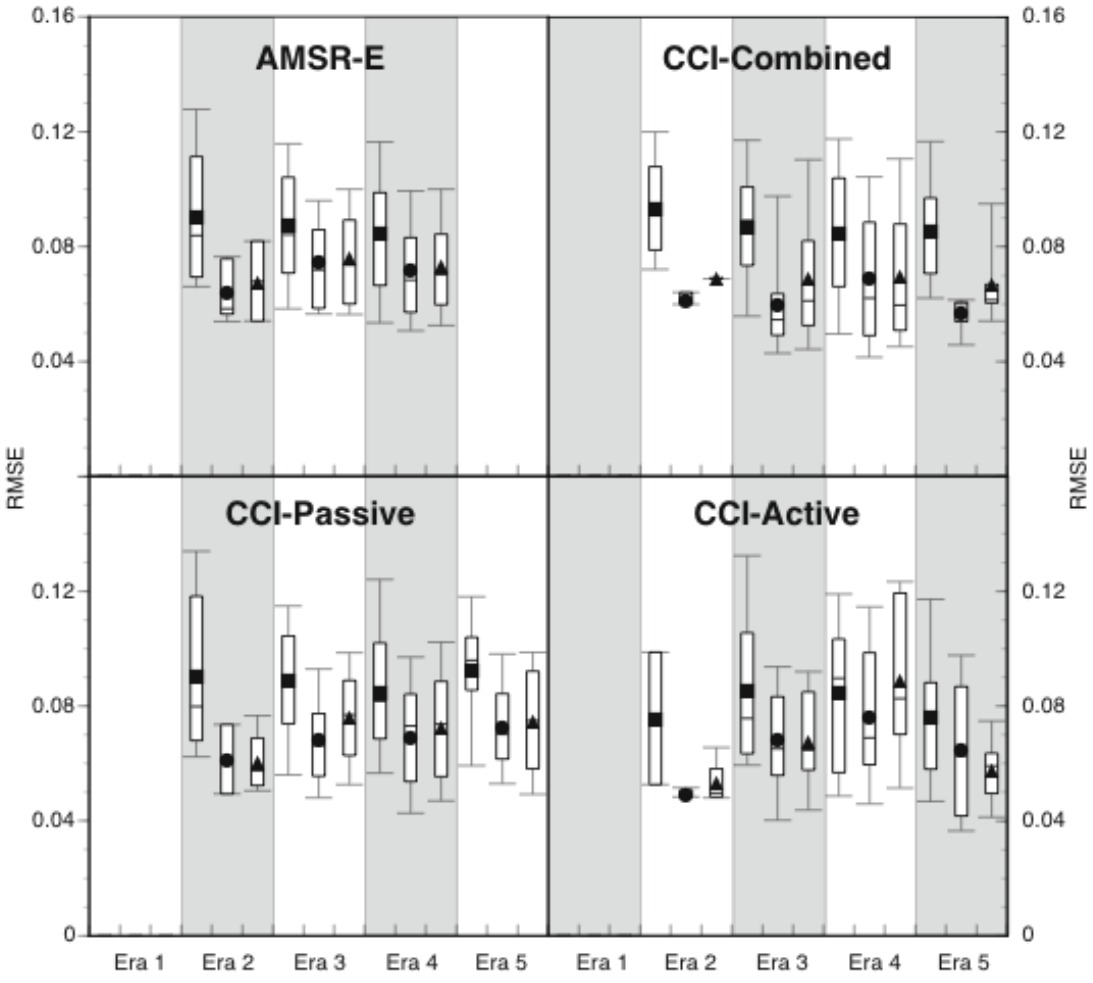
AMSR-E
CCI-Combined
CCI-Passive
CCI-Active
RMSE
RMSE
0.16
0.12
0.08
0.04
0
Era 1
Era 2
Era 3
Era 4
Era 5

Figure 9

639

640

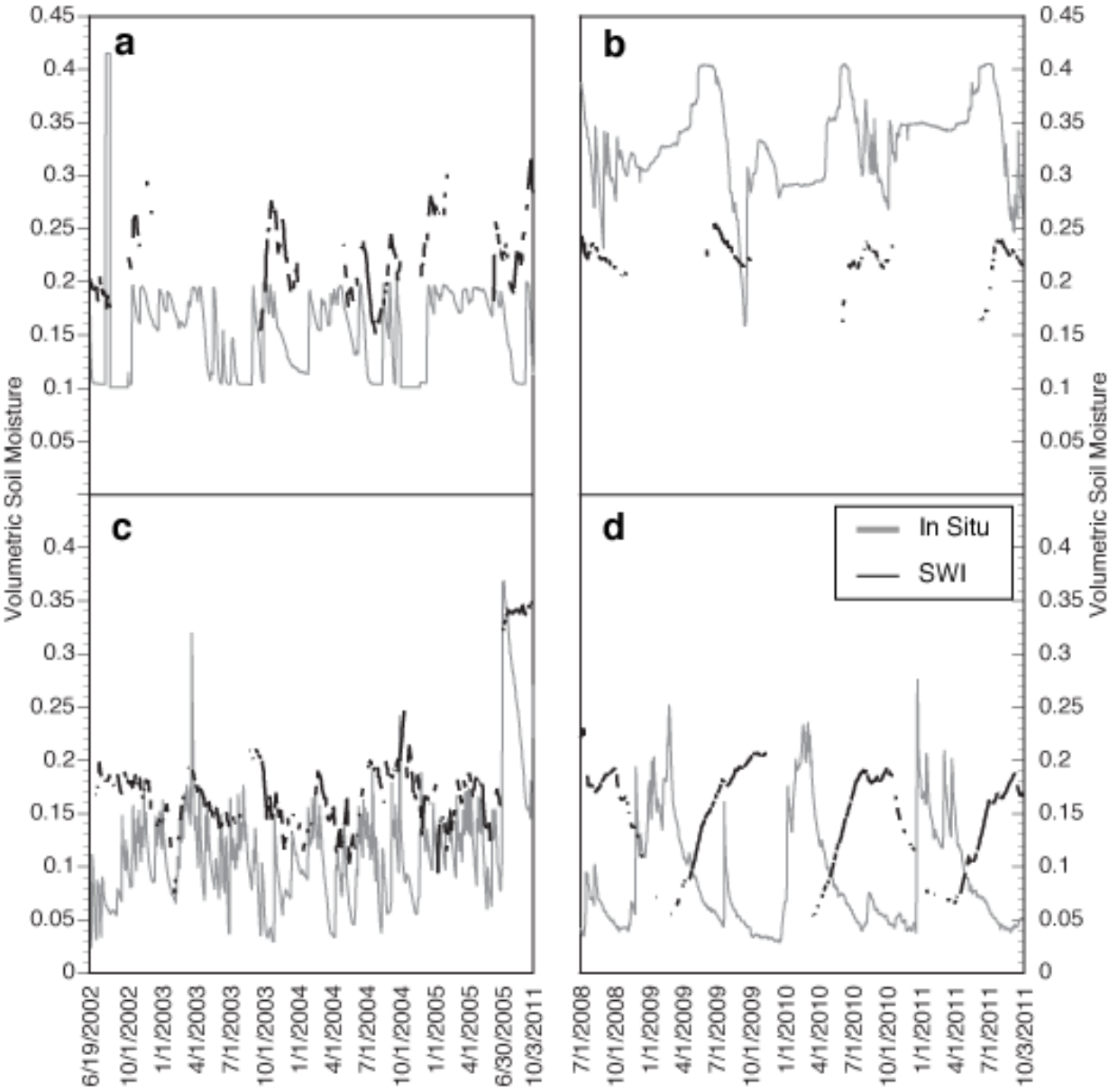

Figure 10

641